Deep learning light field microscopy for video-rate volumetric functional imaging of behaving animal

Zhaoqiang Wang[1,4+], Hao Zhang[1+], Yicong Yang[1+], Guo Li[1], Lanxin Zhu[1], Yi Li[1,3], Mingyang He[1], Tingting Zhu[1], Tzung K. Hsiai[4], Shangbang Gao[3], Peng Fei[1,2*]

[1] *School of Optical and Electronic Information, Huazhong University of Science and Technology, Wuhan, 430074, China.*

[2] *Britton Chance Center for Biomedical Photonics, Wuhan National Laboratory for Optoelectronics, Huazhong University of Science and Technology, Wuhan, 430074, China.*

[3] *College of Life Science and Technology, Huazhong University of Science and Technology, Wuhan, 430074, China.*

[4] *Department of Bioengineering, University of California, Los Angeles, Los Angeles, 90095, U.S.A.*

[+] *These authors contribute equally to this work*

[*] *Correspondence: feipeng@hust.edu.cn*

Abstract

We demonstrate a deep learning-enabled light field microscopy (LFM) to achieve 1 μm -resolution volumetric functional imaging of acting samples at high speed up to 100 Hz. For the raw light field measurement, the use of field detection optics usually limits the recoverable spatial resolution. We develop a deep learning approach to mitigate this limitation and effectively recover a time sequence of higher-resolution 3-D images based on the raw 2-D light field video. Unlike slow iterative LF reconstruction methods, our network approach permits direct inference at video-rate processing throughput (16 volumes per second), which is well suited for sustained volumetric recording of biological dynamics. To obtain optimal network recovery for reconstructing thick specimens, we further use a light-sheet illumination geometry to record high-contrast light field images with less signal overlapping. We demonstrate the success of our approach by *intoto* imaging the neuronal activities of behaving C. elegans and visualizing the cardiovascular hemodynamics inside zebrafish embryo.

Introduction

Light field microscopy (LFM) has recently emerged as a rapid volumetric imaging technique for observing live biological speicimans[1]. Compared to conventional imaging schemes, it captures both the lateral position (x, y) and angle (θ_x, θ_y) of the light reaching the sensor by inserting a microlens array in the native image plane. This enables the camera sensor to record information from a four-dimensional (4-D) light field instead of two-dimensional (2-D) focal plane of the sample in a single snapshot. With obtaining the raw light field information, a series of synthetic focal planes or different perspective views of the sample can be retrieved through post-processing[2-6]. Therefore, light field microscopy eliminates the need of stepwise z-scan which is commonly used for three-dimensional (3-D) microscopy and allows the volumetric imaging of multicellular samples at very high speed. Light field microscopy has delivered promising results for monitoring the transient neuronal activities in various animals, such as *C.elegans*, zebrafish embryo[7,8] and rodent brain[9]. As a reference, it has been proved efficient in brain-wide functional

imaging of a freely swimming zebrafish with a volume rate up to 77 Hz[10].

Although light field imaging has been successful for 3-D imaging of behaving organisms, a tradeoff exists between the high temporal resolution by one exposure and high spatial resolution by which finer structures can be discerned. The limited sensor pixels which are originally allocated to the sampling of 2-D lateral information are now spread over the 4-D light field, resulting in a significant decimation of the lateral resolution. Several attempts have been made to address this problem either through optimizing the way light field being recorded, or developing new algorithms to reconstruct more spatial information from the light field. In terms of recording, a phase mask was incorporated to achieve better LFM resolution profile[11] or a customized dual microlens arrays were placed at the rear pupil plane to record light field in forms of sub-images, which is capable of collecting information from a larger depth[10]. Besides these approaches requiring precise design of customized optics, alternatively, post-processing algorithms, including LF deconvolution[7,12] and enhancement through fusion of ground-truth images[13], has been reported to computationally improve the LF reconstruction quality. These algorithms remain limited to the recovery of sparse signals, and also pose high demand on computation resource for iteratively approaching a high-resolution output. In a more sophisticated method, visual volume reconstruction could be skipped while the neuron signals are statistically demixed directly from the raw light field[8,9]. But this method relies on the signal's fluctuation in time series so that it is insensitive to inactive neurons and incapable of handling moving samples.

Here we propose a novel deep learning strategy to rapidly recover high-resolution volume from a raw LF image. Compared to existing LF techniques, our deep learning-based method achieves better reconstruction quality without compromising LF's advantage in high temporal resolution. We minimize the loss of spatial resolution by incorporating prior structural information of samples so that the network can learn to resolve complex and high-frequency signals from light field. We demonstrate the network's capability by three-dimensionally reconstructing several types of live specimens which are not included the training dataset. Once the LF-deep learning network being well trained, our method can quickly translate one LF frame into a 3-D volume in a few milliseconds, showing significant advantage in time lapsed video processing over those iterative optimization algorithms. To obtain optimal results for reconstructing thick specimens, we further use a light-sheet illumination light field (LSILF) geometry to obtain high-contrast LF raw image with less out-of-focus backgrounds. As demonstrated by the 4-D (3-D space plus time) visualization of acting *C. elegan*s, with using a thick light-sheet to selectively illuminate a 60 μm depth for LF recording, our VCD-LFM method achieves high-fidelity reconstruction of the worm activities at a high resolution of ~ 1 μm and high speed of 16 volumes per second, with an ultra-low computation expense compared to the traditional deconvolution method.

Results

Deep learning light filed reconstruction

We developed VCD-LFM, a deep learning approach which can reconstruct 3-D volumes of quickly behaving samples from its raw 2-D light-field images , at improved spatial resolution and high computation speed. The approach basically includes two stages, the training of the convolutional neural networks and

the inference of the raw light field images, as shown in Fig. 1b. To create the sample data for network training, we first obtained a number of high- resolution (HR) 3-D images of stationary samples (Fig. 1b, step 1). These HR volumes were treated as ground truths in the network. Through the wave optic model of light field microscope[12], these HR images were transformed into a series of corresponding 2-D light-fields, which were used as the input of the neural network (Fig. 1b, step 2). With a View-Channel-Depth (VCD) transformation strategy (Fig. 1b inset) that utilizes the intrinsic mechanism of the multi-channel convolutional neural networks to implement high efficiency light filed deconvolution (LFD), the neural network could produce primary 3-D reconstructions from these simulated light-field inputs (Fig. 1b, step 3). A pixel-wise mean-square-error (MSE) between intermediate 3D reconstructions and ground truths was calculated as the loss function that indicates how different the output is as compared to the ground truth. By iteratively minimizing the loss function using a gradient descent approach (Fig. 1b, step 4), the network gradually get optimized until it could transform the 2-D light-fields into 3-D images that are similar enough to the ground truths. After the training finished, this network was capable of inferring high-quality 3-D images from real 2-D light-field measurements of new behaving samples (Fig. 1b, step 5).These empirical light-fields recorded the sample activity at high volume rate which couldn't be achieved using conventional scanning methods. Based on the prior learning, the network could instantly go through the VCD transform and finish a 3-D light-field reconstruction in milliseconds (Fig. 1b, step 6), reaching a significantly higher spatial resolution as well as imaging throughput as compared to the iterative LFD.

Our VCD-LFM is first characterized by imaging fluorescent point source (~500 nm microbeads) A piece of hydrogel densely embedded with microbeads was simultaneously imaged using both wide-field 3-D scan and LF modes (40X/0.8 objective lens), with HR 3-D volume (ground truth, Fig. 1d, left column) and 2-D LF image being recorded respectively. The LF measurement were recovered into 3-D images by the network (Fig. 1d, right column) and the LFD method (Fig. 1d, middle column), respectively. The lateral and axial resolutions of the reconstructions by each methods are plotted in Fig. 1e. Measured with the full width at half maximum (FWHM) of the bead, Our VCD-LFM has ~1 and 4 μm resolution in lateral and axial dimension respectively, as compared to ~2 (at best) and 4 μm of the LFD result. Furthermore, VCD-LFM circumvents the drawback of nonuniform axial resolution intrinsically brought by LFD method (Fig. 1f), thus free from severe artifacts near the native focal plane. Besides the perceptual comparison, we also use peak signal-to-noise ratio (PSNR), structural similarity (SSIM) and the error map to compare between the two methods (Supplementary Fig. 5), quantitatively providing the evidences that VCD-LFM is able to transform LF projection into 3-D volume with higher fidelity and higher resolution.

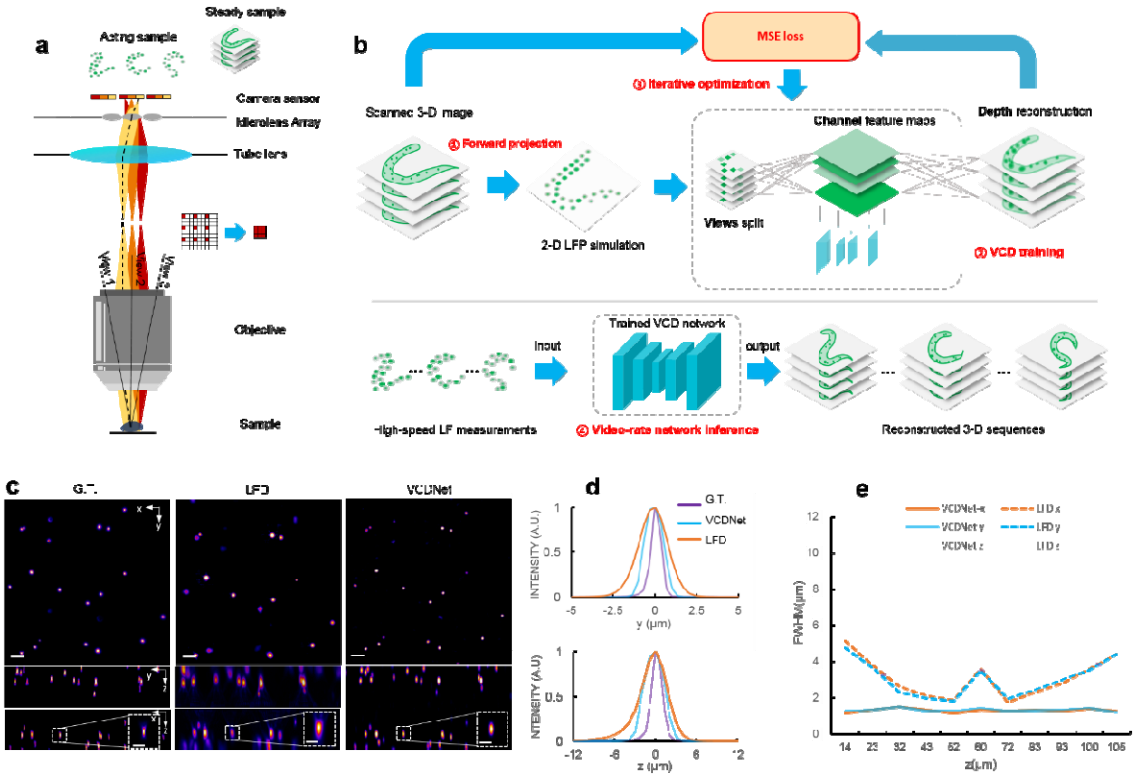

Figure 1. Deep learning light field microscopy procedure. (**a**) Our customized light-field imaging geometry based on an upright microscope. **(b)** The training and inference stage of the network. First, a number of high-resolution 3-D images of stationary samples are obtained (using **a**) as the ground truth (step 1), which are transformed into 2-D LF simulations as the network inputs (step2). The network outputs intermediate 3-D reconstructions (step 3), and compares them with ground truths by pixel-wise MSE. Iteratively minimizing the MSE loss function using a gradient descent approach, the network get trained with optimal parameters that can transform the LF projections into 3-D images similar enough to the ground truths. The inset reveals the view-channel-depth strategy of VCD-LFM. The input light field image is first re-arranged as a stack of views. Then features are extracted and combined from different views, and finally merged into an image volume. Once well trained, the network takes real 2-D LF measurements of new samples as inputs (step 5), and outputs 3-D LF volumes at ultrahigh throughput (step 6). **(c)** Images of fluorescent beads volume. The ground truth is captured by light sheet. A light field image of the same region with selective depth illumination is captured and reconstructed by our VCD-LFM and the traditional LFD, respectively. The results shows as projections of three orientations. (**d**) FWHM of the selected beads from **d** by each method. (**e**).FWHM of the beads at different depth of a 120 um thick volume reconstructed by LFD and VCD-LFM, respectively. Scale bar in d is 10 (x-y) and 2 (vignette in x-z).

Video-rate high-throughput volumetric imaging and reconstruction of behaving C. elegans

We first imaged an anaesthetized transgenic C.*elegans* with mCherry expressed at neuronal cell bodies (Figure 2b-d). 3-D reconstruction of the illuminated volume is given by VCD-LFM network and LFD. Our method delivers a high-quality result with resolution kept on the same level at different depths (Fig. 2b, the

first row). As a comparison, LFD showed a deteriorating trend in deeper region and suffered from a grid-like artifacts near native focal plane (z=0μm) (Fig. 2b, the second row). We also used a wide-field detection with stepwise scanning to record the high-resolution images of the same region of interest (ROI), as the reference to evaluate the quality and fidelity of the reconstructions by the network and LFD. Through identifying neurons at the anterior part, our method shows obviously better ability to correctly discern signals in neuron clusters (Fig. 2c), clearly resolving the worm's neuron structure both in sectioning plane and 3-D rendering (Fig. 2d).

With the promotion of VCD-LFM, we further imaged the activities of behaving RFP labelled *C. elegans* in four dimensions (3-D space + time). A microfluidic chip was designed to encapsulate the C.elegan larva (L2 stage) into a small chamber (300 by 300 μm), thus allowing the worm to freely move within it (Fig. 2a). With employing the high-speed sCMOS camera, sequential LF imaging of the entire behaving larva was performed at a high speed of 100 LF frames per second. The imaging process lasted for 10 seconds with totally 1000 frames recorded. Then the network transformed the recorded LF frames into a time sequence of volumetric images. For a further comparison between our VCD-LFM and the LFD in dynamic imaging, a single LF frame is recovered by both methods respectively (Fig.2f). VCD-LFM accurately resolves the dense neuron signals in the anterior part with far better resolution in both lateral and axial directions than the LFD. The VCD-LFM becomes even more competitive when processing the time sequence, being able to reconstruct the whole 1000 LF frames in one minute, at a maximum speed of 16.5 volumes per second (1000 times faster than LFD). As for the LFD, such video rate reconstruction is by no means possible due to the iterative computation (Fig. 2g). The volumetrically reconstructed activities of the acting worm at five different time points are projected along depth and shown in Fig. 2h. The color merging of reconstructed volumes at 3 adjacent time points (0ms, 50ms and 100ms) indicates the moving tendency of different body parts (Fig.2h). The success in the volumetric imaging of behaving C.elegans reveals that VCD-LFM could be well suited for sustained video imaging of biological dynamics in three dimensions, which is very computationally challenging to conventional LFM reconstruction methods or other microscopy techniques.

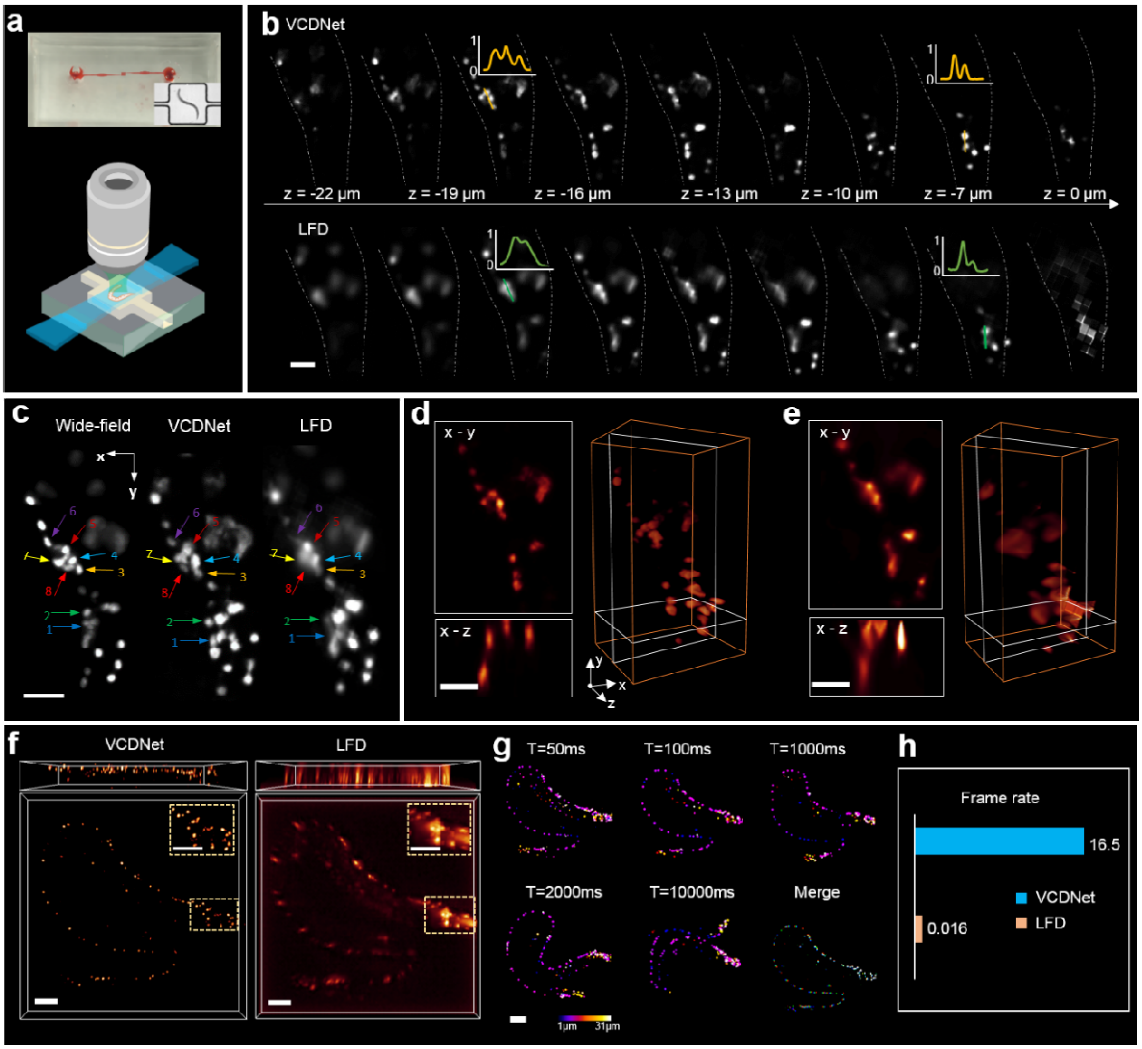

Figure 2. VCD-LFM Imaging of C.elegans. (**a**) The micro-fluidic chip for living C.elegans imaging. A real picture of the chip (top) and its chamber (vignette) as well as a sketch of the imaging setup (bottom) is given. (**b**) Volumetric reconstruction by our method and LFD, from single exposure (20ms) of light-field microscope. The worm was placed off the native focal plane of the objective and a 30 thick volume was selectively illuminated by light sheet. The LFD result was generated after 8 iterations. Two intensity profiles of color lines at two plane (-18µm and -7µm) are drawn for each method. (**c**) Maximum intensity projection (MIP) of planes of b for a clear illustration of our method's ability to discern dense signals. Arrows and numbers give examples of neurons which actually exist in wide-field (left) and resolved by our method (middle) but blurred by LFD (right). Wide-field image was captured using a scanning method for the same ROI but at a different time. A little deformation was caused by movement of worm. Slice of deconvolution at native focal plane is deliberately excluded for better visualization without pixel blocks, which can be noticed in b. (**d**) A 3D rendering and two cross sections of worm's tail by our method, (**e**) The same sample as **d** via LFD. (**f**)Top and side views of the reconstruction of live C.elegans in the microfluidics chip at T=0ms using our method (left) and LFD (right). Upper right inset shows densely signal in the anterior region. (**g**) Projections along depth of reconstructions by our method at different time points. The lower right one is the color merge of 3 adjacent time points, 0 ms (red channel), 50 ms(green channel) and 100ms (blue channel), indicating the tiny displacement our

neural cells resolved by our method. (**h**)The computational speed (frame rate) comparison between our method and LFD. Scale bar, 10μm in (**b**) (**c**) (**d**), 20 μm in (**f**) (**g**).

Heart Dynamics Imaging

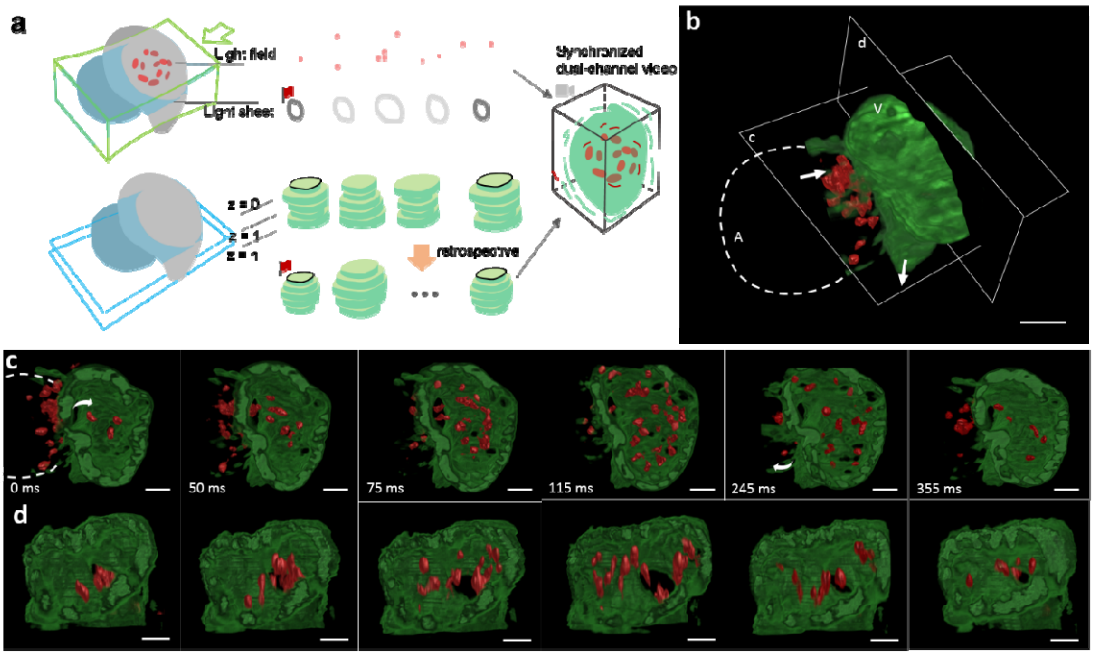

Figure 3 4-D imaging of blood flow and beating heart in zebrafish using hybrid system of light-field and light-sheet microscope. (**a**) Schematic of images acquisition and reconstruction process. Sequence of 3-D Red blood cells (RBCs) and 2-D section of cardiomyocytes were recorded simultaneously with light-field and light-sheet detections, respectively, under volumetric (532 nm) and planar (473 nm) illumination. Then, movie stacks of myocytes were acquired at different depths under planar (473 nm) illumination. Each movie contains 3-5 cardiac cycles. Finally, light-field and light-sheet images were post-synchronized together. (b) 3D visualization of cardiomyocytes (cmlc2::GFP) and RBCs (gata1a::dsRed). Arrows indicate the direction of blood flow, from the AV canal to outflow tract. Dotted line marks the region of atrium. A: atrium; V: Ventricle. Scale bar, 40 μm. (**c,d**) 4-D bisected heart using sectioning planes indicated in (b). Myocytes were synchronized with blood blow using the periodic movement of heart wall. Dotted line indicates the region of atrium. Scale bar, 30 μm.

Methods

Imaging Setup

The light field / wide-field dual mode microscope with selective depth illumination function was built on an Olympus BX51 upright microscope. The customized laser-sheet illumination arm, piezo sample control stage (P12.Z200K, Coretomorrow), and water imaging chamber were directly integrated on the microscope stage. A 40X/0.8-NA water objective (Olympus, LUMPlanFLN) was used to collect the fluorescence emissions. The LF/WF detection arm is appended to the camera port of host microscope, with using a flip

mirror to switch between the two detection modes. The microlens array (OKO Optics, 40K elements) is placed at the native image plane of the LF detection path, projecting the angular light-field signals onto a sCMOS camera (Hamamatsu Flash 4.0).

Light-field microscope setup with selective depth illumination

The LF imaging were carried out using a homebuilt light-field microscope with features of microlens array (MLA) wavefront sensing and selective depth illumination. The optical setup of the microscope was shown in Fig.1a and supplementary. The MLA (Thorlabs) was placed at the native image plane to modulate the light so that a 4D light-field could be projected onto a 2D image sensor (Hamamatsu, Flash 4.0 V3). In addition to the conventional epi-illumination mode, we also included a laser-sheet illumination to optically sectioning the thick sample at selective depth. This selective illumination mode restricts the fluorescence excitation within an axial region which is matched to the re-focusable depth of the LF detection. Compared to conventional Selective Plane Illumination Microscopy[14,15] (SPIM) where a thinner light-sheet illumination (usually less than 10 μm) is required for achieving high z-axis resolution, the selective depth illumination in light-field microscope stressed more on the elimination of the background contamination brought by the unnecessary signals beyond the re-focusable region of the light field. Thus, it could produce high-quality LF image with increased contrast, especially for thick and scattering medium, as shown in Fig. 1c. Moreover, in our setup, the axial extent of the laser-sheet was tunable from 4 to 30 μm so that 3D SPIM and 2D light field imaging could be both implemented on the stationary reference samples. Correspondingly, a switchable wide-field detection was built in parallel with the light-field paths, allowing the system to obtain regular HR 3-D image by stepwise z-scan. It is also noteworthy that light-field reconstruction is mainly an inverse problem based on a theoretical optic model, or point spread function (PSF) of the system. When using conventional wide-field illumination, as a limited computation resource restricts our consideration to a certain subset of entire PSFs, signals undefined in our model will lead to artifacts and false reconstruction. A light-sheet illumination in this case optimizes the reconstruction problem by confining the excited signals in a selective volume that can be fully included in computation model (Supplementary).

Implementation of deep learning light field reconstruction algorithm

VCD strategy

In a general convolutional neural network (CNN), the output channels of each convolutional layer represent feature maps extracted by different convolution kernels, which then flows to the next layer as the input to further distill the features. In this way, the network generates a multi-channel output where each channel is a non-linear combination of the original input channels. This mechanism intrinsically agrees with the light field deconvolution: each axial slice of the reconstruction volume arises from a superposition of all angular views of light field projection (LFP), after convolved with the corresponding point spread function (PSF). Thus in our proposal, a View-Channel-Depth (VCD) transformation is naturally used to reconstruct a 3-D volume with depth information from a bunch of angular views of light field images.

Though the program takes a 2-D LFP as the input, the very first convolutional layer of our net actually deals with a re-formatted 3-D ([height, width, views]) data, in which the 3rd dimension is the extracted and successively arranged angular views from the raw input. The first VCD layer abstracts

feature maps from all these views, making the initial transformation from “view” to “channel”. The following convolutional layers keep combining old channels from previous layer and generating new ones, to fully excavate the hidden features. The last layer, finally gives a 3-D output, of which the 3rd dimension is still composites of channels from its predecessor but with a channel number that equals to the depth of the 3-D image to be reconstructed, fulfilling the second transformation from “channel” to “depth”.

Network Structure

Our network comprises an up-scaling part and a feature extracting part (i.e. the VCD transformation module). The former interpolates the angular views to the same lateral size as the LFP. The latter is adapted from the U-net architecture and made up with several convolution layers and deconvolution layers. Each convolution layer and deconvolution layer has three parameters: n, f and s, denoting the output channels number of this layer, the filter size of convolution kernel and the lateral step size when kernel moves, respectively. A convolution layer with s = 2 halves the lateral size of feature maps, while a deconvolution layer with s = 2 will double it. The arrow between two layers stands for a concatenating operation that put the feature maps of these two layers together, as the input to the follow-up layers.

C. elegans experiments

To map the neurons in C.*elegans*, we chose worms at young adult stage while stain used in this study was: QW1217 hpls491(Prgef-1::GCaMP6); hpls467(Prab-3::NLS-RFP). It was maintained at 22 ℃ on NGM plates with OP50 E.coli as food. The worm was immobilized by levamisole and further embedded in 1% agarose. We generated a 30um-thick light sheet and moved the focal plane of objective to the bottom of light sheet so the illumination region spanning from -30um to 0um. The worm was then placed in this region by a z-axis stage motivated by the actuator [ZST225B, Thorlabs] to make the neurons perfectly excited while the background was greatly eliminated to improve contrast. We used a 40X water objective and a standard RFP filter set. For each worm, we first captured light field image, and then quickly switched to normal widefield detection, scanned the worm body for a reference for light field reconstruction result.

In prior to reconstruction, a network model should be well trained. We collected the static high-resolution 3D images through a confocal laser scanning microscope [FLUOVIEW FV3000, Olympus]. The samples are worms of the same strain as previously discussed and also immobilized. We randomly imaged about 24 worms under 40X magnification and transformed them into simulated light field raw images through a wave optic model[12]. Then we trained our network through pairs of light field image and corresponding 3D images until the loss function is stabilizing. Finally we saved the network for all the empirical data reconstruction. After reconstruction, we map the neurons in C.*elegans* with the reference of WormAtlas.

Fish husbandry and lines

Zebrafish (Danio rerio) were bred and maintained at the UCLA Core Facility, and experiments were performed in compliance with UCLA IACUC protocols . Transgenic lines Tg(cmlc2:gfp), Tg(gata1a:dsRed) were used. The two lines were crossbred and micro-injected with gata2a morpholino oligonucleotide to reduce hematopoiesis, thereby, resulting in a mild reduction in the number of red blood cells. Embryos were maintained until 4dpf (days post fertilization) in standard E3 medium supplemented with PTU (Sigma

Aldrich, MO) at 28.5 ℃ to inhibit melanogenesis. Then, the embryos were immobilized with tricaine (3-amino benzoic acidethylester, Sigma Aldrich, MO) and embedded in 1% low-melting-point agarose inside FEP (Fluorinated Ethylene Propylene) tube for further imaging.

Zebrafish heart imaging

For the movement of red blood cells in three dimensions, the middle of ventricle was moved to the focal plane thereby the light-block(532nm) could cover the entire heart while a light-sheet(488nm) shed an optic sectioning inside the ventricle. A movie of light-field images was acquired to trace the red blood cells while a time sequence of 2-D section plane of myocytes was recorded concurrently to provide temporal reference for synchronization afterwards.

A movie stack of light-sheet images was then acquired consisting 60-70 movies with a z spacing of 2 µm, to recover the myocardial structures. We used up to 512 x 512 camera pixels which yields a lateral FOV of 166 µm x 166 µm. Both light-field and light-sheet movies covered 3-4 cardiac cycles within a 5 ms exposure time.

To reconstruct the blood flow from light-field, we trained the LFRNet on confocal images of static red blood cells. A light-field PSF that matched the parameters of the imaging system was chosen when generating the synthetic light-field images, which yielded 101 distinct z planes at step of 2 µm spanning from -50 µm to 50 µm of the focal plane. The model was trained on [The computation consumption needed future experiment on new workstation.]

The synchronization for light-field and light-sheet images was conceptually based on algorithms as previously described [1,2]. Here we customized it for our dual-modality system in which the 2-D time sequence of myocytes recorded simultaneously with light-field movies will be taken into the synchronization scheme along with the light-sheet movie stack captured subsequently. And it will function as temporal markers to map the cardiomyocytes from light-sheet to the blood flow from light-field.

[Here I can also talk about spatial registration, which are just some little tricks if people want to repeat the experiments]

The imaging experiments were automated by customized LabVIEW program and the synchronization code was implemented in Matlab.

Funding

National Key R&D program of China (2017YFA0700500), Research Program of Shenzhen (JCYJ20160429182424047), the National Natural Science Foundation of China (21874052, and 31671052), the National Science Foundation of Hubei (2018CFA039), Wuhan Morning Light Plan of Youth Science and Technology (2017050304010295) and the Junior Thousand Talents Program of China (Peng Fei and Shangbang Gao).

Acknowledgements

We thank Haiwen Li, Lanxin Zhu, Guo Li for technical assistance. We thank Yanyi Huang for discussions and comments on the manuscript,

Disclosures

The authors declare that there are no conflicts of interest related to this article.

References

1 Levoy, M., Ng, R., Adams, A., Footer, M. & Horowitz, M. in *ACM SIGGRAPH 2006 Papers* 924-934 (ACM, Boston, Massachusetts, 2006).

2 Levoy, M., Ren, N., Adams, A., Footer, M. & Horowitz, M. 924-934.

3 Hoffmann & Maximilian. Light field deconvolution microscopy for optical recording of neuronal population activity. (2014).

4 Pégard, N., Liu, H. Y., Antipa, N., Waller, L. & Adesnik, H. in *Imaging Systems and Applications.* JTh4A.3.

5 Pégard, N. C. *et al.* Compressive light-field microscopy for 3D neural activity recording. *Optica* **3**, 517 (2016).

6 Prevedel, R. *et al.* Simultaneous whole-animal 3D-imaging of neuronal activity using light-field microscopy. *Nature Methods* **11**, 727-730 (2014).

7 Prevedel, R. *et al.* Simultaneous whole-animal 3D imaging of neuronal activity using light-field microscopy. *Nature Methods* **11**, 727, doi:10.1038/nmeth.2964 https://www.nature.com/articles/nmeth.2964#supplementary-information (2014).

8 Pégard, N. C. *et al.* Compressive light-field microscopy for 3D neural activity recording. *Optica* **3**, 517-524, doi:10.1364/OPTICA.3.000517 (2016).

9 Nöbauer, T. *et al.* Video rate volumetric Ca2+ imaging across cortex using seeded iterative demixing (SID) microscopy. *Nature Methods* **14**, 811, doi:10.1038/nmeth.4341 https://www.nature.com/articles/nmeth.4341#supplementary-information (2017).

10 Cong, L. *et al.* Rapid whole brain imaging of neural activity in freely behaving larval zebrafish (Danio rerio). *eLife* **6**, e28158, doi:10.7554/eLife.28158 (2017).

11 Cohen, N. *et al.* Enhancing the performance of the light field microscope using wavefront coding. *Opt. Express* **22**, 24817-24839 (2014).

12 Broxton, M. *et al.* Wave optics theory and 3-D deconvolution for the light field microscope. *Opt. Express* **21**, 25418-25439, doi:10.1364/OE.21.025418 (2013).

13 Lu, C. H., Muenzel, S. & Fleischer, J. in *Frontiers in Optics.*

14 Jan, H., Jim, S., Filippo, D. B., Joachim, W. & Stelzer, E. H. K. Optical sectioning deep inside live embryos by selective plane illumination microscopy. *Science* **305**, 1007-1009 (2004).

15 Huisken, J. & Stainier, D. Y. R. Selective plane illumination microscopy techniques in developmental biology. *Development* **136**, 1963-1975 (2009).